Journal for ImmunoTherapy of Cancer

Pharmacological tumor PDL1 depletion with chlorambucil treats ovarian cancer and melanoma: improves antitumor immunity and renders anti-PDL1-resistant tumors anti-PDL1-sensitive through NK cell effects

Haiyan Bai,[1] Alvaro S Padron,[2] Yilun Deng,[2] Yiji J Liao,[1] Clare J Murray,[3,4] Carlos Ontiveros,[1,4] Suresh J Kari,[1] Aravind Kancharla ,[5] Anand V R Kornepati,[4] Myrna Garcia,[4,6] Ryan Michael Reyes ,[4,6,7] Harshita B Gupta ,[2] Jose R Conejo-Garcia,[8] Tyler Curiel [1,4,6,9]

To cite: Bai H, Padron AS, Deng Y, *et al*. Pharmacological tumor PDL1 depletion with chlorambucil treats ovarian cancer and melanoma: improves antitumor immunity and renders anti-PDL1-resistant tumors anti-PDL1-sensitive through NK cell effects. *Journal for ImmunoTherapy of Cancer* 2023;**11**:e004871. doi:10.1136/jitc-2022-004871

► Additional supplemental material is published online only. To view, please visit the journal online (http://dx.doi.org/10.1136/jitc-2022-004871).

Accepted 18 October 2022

For numbered affiliations see end of article.

Correspondence to
Dr Tyler Curiel;
tyler.j.curiel@dartmouth.edu

ABSTRACT

Background Tumor intracellular programmed cell death ligand-1 (PDL1) mediates pathologic signals that regulate clinical treatment responses distinctly from surface-expressed PDL1 targeted by αPDL1 immune checkpoint blockade antibodies.

Methods We performed a drug screen for tumor cell PDL1 depleting drugs that identified Food and Drug Administration (FDA)-approved chlorambucil and also 9-[2-(phosphonomethoxy)ethyl] guanine. We used in vitro and in vivo assays to evaluate treatment and signaling effects of pharmacological tumor PDL1 depletion focused on chlorambucil as FDA approved, alone or plus αPDL1.

Results PDL1-expressing mouse and human ovarian cancer lines and mouse melanoma were more sensitive to chlorambucil-mediated proliferation inhibition in vitro versus corresponding genetically PDL1-depleted lines. Orthotopic peritoneal PDL1-expressing ID8agg ovarian cancer and subcutaneous B16 melanoma tumors were more chlorambucil-sensitive in vivo versus corresponding genetically PDL1-depleted tumors. Chlorambucil enhanced αPDL1 efficacy in tumors otherwise αPDL1-refractory, and improved antitumor immunity and treatment efficacy in a natural killer cell-dependent manner alone and plus αPDL1. Chlorambucil-mediated PDL1 depletion was relatively tumor-cell selective in vivo, and treatment efficacy was preserved in PDL1KO hosts, demonstrating tumor PDL1-specific treatment effects. Chlorambucil induced PDL1-dependent immunogenic tumor cell death which could help explain immune contributions. Chlorambucil-mediated PDL1 reduction mechanisms were tumor cell-type-specific and involved transcriptional or post-translational mechanisms, including promoting PDL1 ubiquitination through the GSK3β/β-TRCP pathway. Chlorambucil-mediated tumor cell PDL1 depletion also phenocopied genetic PDL1 depletion in reducing tumor cell mTORC1 activation and tumor initiating cell content, and in augmenting autophagy, suggesting additional treatment potential.

Conclusions Pharmacological tumor PDL1 depletion with chlorambucil targets tumor-intrinsic PDL1 signaling that mediates treatment resistance, especially in αPDL1-resistant tumors, generates PDL1-dependent tumor immunogenicity and inhibits tumor growth in immune-

WHAT IS ALREADY KNOWN ON THIS TOPIC

⇒ Tumor surface PDL1 mediates immunopathology by inhibiting PD1-expressing antitumor immune cells. Tumor cell-intrinsic PDL1 mediates non-canonical immunopathology that is often not affected by immune checkpoint blockade (ICB) antibodies. Chlorambucil kills tumors by damaging their DNA. Generally, reduced tumor PDL1 makes αPDL1 ICB work less effectively.

WHAT THIS STUDY ADDS

⇒ We show that tumor cell-intrinsic PDL1 can be pharmacologically depleted to reduce its immunopathological potential and that some effects are not replicated by αPDL1. In fact, pharmacological PDL1 reduction can make αPDL1-unresponsive tumors become αPDL1-responsive. Chlorambucil mechanisms of action include depleting tumor cell PDL1 content and improving natural killer cell-mediated tumor control, and can work in a tumor PDL1-dependent manner. Chlorambucil induces immunogenic cell death in a tumor PDL1-dependent manner but only in selected cancers.

HOW THIS STUDY MIGHT AFFECT RESEARCH, PRACTICE OR POLICY

⇒ Chlorambucil could be used to reverse ICB unresponsiveness in selected cancers, addressing an important, unmet medical need. It is FDA approved and thus could be tested clinically for anticancer activity alone or in combination treatments rapidly.

dependent and independent manners. It could improve treatment efficacy of selected agents in otherwise treatment-refractory, including αPDL1-refractory cancers, and is rapidly clinically translatable.

BACKGROUND

Programmed death ligand 1 (PDL1, CD274), an immune cosignaling molecule in the B7-homology family, interacts with its receptor PD1 on T cells to attenuate antitumor T cell responses, allowing tumors to escape immune surveillance.[1 2] Blocking PDL1 signals with antibodies is the basis for highly effective immune checkpoint blockade (ICB) therapy that mediates anticancer efficacy, but only in a minority subset of patients.[2–5] Tumor-extrinsic effects of PDL1 have been intensively studied. However, it is now clear that PDL1 also mediates important tumor-intrinsic signaling that promotes pathological outcomes including treatment resistance, reviewed in reference.[6] Genetic tumor PDL1 depletion reverses pathological tumor-intrinsic signals to improve treatment efficacy of small molecules and cytotoxic agents[7–10] and deletion of the PDL1 cytoplasmic tail in tumor cells can improve ICB efficacy.[11 12] To overcome difficulties in translating genetic approaches to tumor PDL1 depletion, we screened libraries of agents that were enriched for FDA-approved drugs for PDL1 depletion efficacy that identified chlorambucil, a DNA alkylating nitrogen mustard drug approved to treat chronic lymphocytic leukemia and other neoplasms,[13 14] as an agent that reduces cancer cell PDL1 and thus could be used clinically as a pharmacological means to reduce deleterious tumor-intrinsic PDL1 signals. We also identified 9-[2-(phosphonomethoxy) ethyl] guanine (PMEG) as a tumor PDL1 depletion agent, but did not study it in detail as it is not FDA approved.

We show that chlorambucil-mediated tumor PDL1 depletion was through distinct mechanisms in different cancer cell lines. In vivo, chlorambucil controlled tumor growth in mouse melanoma and ovarian cancer models in a tumor PDL1-dependent manner, independent of host PDL1 expression. It also paradoxically rendered otherwise αPDL1-refractory tumors to be αPDL1-responsiveness in vivo through a natural killer (NK) cell-dependent mechanism and improved antitumor immunity in a NK cell-dependent manner, which is a likely efficacy mechanism. Chlorambucil-mediated tumor PDL1 depletion phenocopied important genetic PDL1 depletion effects in vitro, including suppressing tumor mTORC1 signals and stemness, suggesting additional potential uses and mechanisms for treatment efficacy meriting additional studies. Our study suggests a novel strategy to reprogram the tumor for ICB treatment response by pharmacological tumor PDL1 signal reduction with potential additional clinical applications, requiring additional work to achieve this objective. As chlorambucil is FDA approved, orally available and generally tolerable at doses required for these effects, approaches shown can be rapidly tested clinically.

MATERIALS AND METHODS

Generation of murine PDL1-red fluorescent protein construct and tumor cell expression

The pLVX-DsRed-Express2-N1 lentiviral vector was purchased from Clontech (Mountain View, California, USA, cat. 632560). pLVX-DsRed-mPDL1-red fluorescent protein (RFP) expression vector conjugating RFP to the PDL1 C-terminus was generated by PCR cloning using a murine PDL1 expression vector as a backbone (ORIGENE, cat. MG203953), using the primers PDL1-AA259F-5'-gcagatagttccctcgaggccaccatgttcttgagaaaacaag tgaga-3'; PDL1-AA290R-5' agggttcaacagaattcgcgtctcctc-gaattgtgtatcatttcg-3'. Amplified PCR product was cloned into pLVX-DsRed-Express2-N1 vector using Xho-1 and EcoR1 sites. PDL1-C terminus plasmid sequence and orientation was confirmed by sequencing. Lentivirus was produced by transfecting HEK293T cells with pLVX-DsRed-mPDL1-Cterminus-RFP plasmid with packaging vectors pMD-2G, pMDLg/pRRE and pRSV-Rev plasmids (cat. 12259, 12253, 12251, Addgene) using Turbofect Transfection Reagent (Thermo Fisher, Waltham, Massachusetts, USA) according to manufacturer protocols. The lentivirus-containing supernatants were collected and concentrated using Lenti-X (Takara). Transduction was by adding the lentivirus to medium followed by puromycin (1 µg/mL) selection for 14 days. Pooled clones were selected and expression of PDL1-C terminus-RFP was confirmed by flow cytometry for RFP expression and Western blotting.

High-throughput drug screen to identify PDL1 depleting drugs

We selected a subline suitable from PDL1 RFP reporter cells described above for drug screens by flow cytometric sorting for RFP^{hi} cells. PDL1 RFP reporter cells were seeded at 800 cells/well into 384 well black µ-clear film plates, Griener bio-one plates, (Kremsmünster, cat. 781091) using the EL406 Washer/Dispenser (Biotekin 50 µL medium. Plates were incubated overnight at 37°C, 5% CO_2 and then treated with 2.5 µM and 10 µM compounds from the Prestwick and 10 µM from the LOPAC library (1200 compounds in each library that are largely in human trials or FDA approved) using the Agilent Bravo liquid pipetting platform and incubated for 48 hours. Cells were then washed with phosphate-buffered saline (PBS), and fixed with 4% paraformaldehyde (Electron Microscopy Sciences, cat.15714S) and labeled with 2 µg/mL 4′,6-diamidino-2-phenylindole (DAPI), (Molecular Probes, cat. D1306) and 1 µg/mL Cell Mask-Blue (Invitrogen, cat. H32720). Plates were then imaged using the Operetta High Content Imaging System (Perkin Elmer) in the DAPI and Cell Mask Blue (excitation 360–400 µM, emission 410–480 µM), and RFP channel (excitation 520–550 µM, emission 560–630 µM). Images were analyzed using Perkin Elmer Harmony Software. Briefly, the number of cells in vehicle (DMSO) treated or compound-treated wells were binned into 6 RFP expression level segments based on per cell mean fluorescent intensities of RFP expression. Compounds

that induced >2.6 fold PDL1 reduction versus control DMSO with >80% viability were identified as potential hits. The Cell Mask Blue stain allowed for analysis of cell shape and size and the DAPI stain allowed for analysis of nuclear shape, nuclear size and nuclear fluorescence intensity to exclude cells if these parameters were altered.

Cell lines and in vitro treatments

Human OVCAR5 ovarian cancer cells were obtained from Dr. David Curiel, Washington University. Mouse B16-F10 melanoma (herein 'B16') and human ES2 ovarian cancer cells were purchased from the American Type Culture Collection. ID8agg mouse ovarian cancer, ID8agg-Luc, PDL1^{lo} ID8agg and PDL1^{KO} B16 cells were generated as we described.[7 15] All cell lines were negative for *Mycoplasma* in periodic testing using MycoAlert Mycoplasma Detection Kits (Lonza, cat. LT07-318), according to manufacturer directions and used in passages <5. Mouse lines were maintained in 5% fetal bovine serum (FBS)-containing RPMI-1640 medium (Roswell Park Memorial Institute). Human lines were maintained in 10% FBS-containing Gibco Dulbecco's Modified Eagle medium, all supplemented with 1% penicillin/streptomycin, 1% L-glutamate, and 1% 4-(2-hydroxyethyl)−1-piperazine ethane sulfonic acid. Cells were treated with chlorambucil (Sigma, cat. C0253), gemcitabine (Sigma, cat. G6423), rabusertib (Selleckchem, cat. S2626), MG132 (Sigma, cat. M7449) or extracellular growth factor (Thermo Fish, cat. PHG0313) at indicated concentrations.

Cell proliferation and viability assays

Cells (500/well) were plated in 96-well flat-bottom plastic culture plates in 100 µL medium and treated with chlorambucil at indicated concentrations for 48 hours. Cell viability was determined by a cell counting kit-8 (CCK-8 (MedChemExpress; cat. HY-K0301). Absorbance was measured at 450 nm using a BioTek Synergy 2 Multi-Mode Plate Reader. Proliferation was assessed in triplicate in three separate experiments for all in vitro data shown.

In vivo tumor challenge, treatments and assessments

Wild-type C57BL/6 mice, NSG (NOD-SCID IL2Rgamma^{null}) mice were purchased from Jackson Labs and PDL1^{KO} mice on the C57BL/6 background were a kind gift from Dr. Leiping Chen, then at Mayo Clinic. Mice were bred in our animal facility and used at 7–20 weeks old. All mice were given ad libitum water and food and housed under specific pathogen-free conditions and matched for sex and age in each experiment. 5×10^5 B16 or PDL1^{KO} B16 cells in log growth phase in 0.15 mL sterile PBS were given subcutaneously (both sexes). 4×10^6 ID8agg-Luc or PDL1^{lo} ID8agg cells in log growth phase were given intraperitoneally to females only. For NSG mice, 1.5×10^5 B16 or 1×10^6 ID8agg cells were used. Intradermal tumor growth was measured with Vernier calipers and volume was calculated as (length × width^2)/2. Intraperitoneal ID8agg-Luc tumor growth was determined by IVIS Lumina Imaging System (Perkin Elmer) 15 min after intraperitoneal injection of 3 mg PBS-dissolved d-luciferin K+ (Gold Biotechnology) with 1 min exposure, medium binning, and F/stop=1. Identical regions of interest were drawn over each subject's abdomen and average radiance (photons/sec/cm^2/sr) was quantified with Living Image software version 4.2. Body weight was determined weekly for PDL1^{lo} ID8agg tumor and percentage increase body weight was used as a surrogate for tumor as we reported.[16] Tumors were collected and weighed at sacrifice in confirmation. Survival was determined as spontaneous death, moribundity, tumor volume >1500 mm^3 for subcutaneous tumor, or weight >130% of baseline (ascites) in ID8agg or >120% for PDL1^{lo} ID8agg tumors. One chlorambucil cycle is 5 consecutive daily intraperitoneal injections injections using 27 gage needles (BD, cat. 305136) in 150 µL PBS, followed by 2 days of rest (doses optimized for each tumor and treatment condition in preliminary assessments as indicated) versus respective vehicle control injections. Two treatment cycles were used for B16 or PDL1^{KO} B16, and three treatment cycles for ID8agg or PDL1^{lo} ID8agg starting 7 days after tumor cell challenge. αPDL1 (clone 10F.9G2, BioXcell) or respective isotype control was injected intraperitoneally at 100 µg/mouse every 4 days starting on day 7 after tumor challenge for times indicated. To rechallenge cured mice, WT mice that were PDL1^{lo} ID8agg tumor-free >100 days after initial challenge were rechallenged with 4×10^6 ID8agg cells. Age matched naïve WT mice were challenged as controls. Tumor volume and mice survival were measured as above.

Flow cytometry

Mice were sacrificed by cervical dislocation after induction of deep isoflurane anesthesia. Tumors and ascites were collected and cells were stained as we described.[15] Cells were stained with antibodies from Invitrogen: αCD45 (30-F11); Biolegend: αCD3 (17A2), αCD11C (N418), αNK1.1(PK136), αCXCR5 (L138D7), αGr-1 (RB6-8C5), αGranzyme B (QA16A02), αTim3 (B8.2C12), αCD62L (MEL-14), αCD31 (390), αCD44 (IM7), αCD24 (M1/69), αCD133 (315–2C11); BD Bioscience: αCD8 (53–6.7), αCD4 (GK1.5), αB220 (RA3-6B2), αIFNγ (XMG1.2), αPDL1 (MIH5), αCCR2 (475301), αCD25 (PC61), αTCF-1 (S33-966); Tonbo: αCD11b (MI/70), αFOXP3 (3G3) and Thermo Fisher: αPD1 (J43) plus matched isotype controls. We used Alexa Fluor antibody labeling kit (cat. A20186, Thermo Fisher) to add fluorescence to αFAP (ab28244, Thermo Fisher). Apoptosis assessment used Annexin V and propidium iodide (Thermo Fisher Scientific, cat. V13245) according to manufacturer instruction. Data were acquired on LSR II or Cytek Aurora hardware and analyzed by FACS Diva (BD Bioscience) or FlowJo software (Flow Jo).

To study immunogenic cell death, cells were treated with chlorambucil with indicated doses and time, harvested, washed and cell suspensions were adjusted to 2×10^6 cells/mL in 200 µL ice-cold PBS, 10% FCS, 1% sodium azide. We added 2 µL anti-Calreticulin antibody (ab209577) or isotype control rabbit IgG antibody

(ab209478) per sample, incubated cells for 30 min in the dark at 4°C, washed cells three times by centrifugation at 400 g for 5 min and resuspend them in 300 µL in ice-cold PBS, 10% FBS, 1% sodium azide. We fixed samples with 1% PFA for immediate analysis.

Annexin V/propidium iodide staining

We harvested cells after incubation, washed in cold PBS, recentrifuged cells, discarded supernatant and resuspended in 1X Annexin-binding buffer at~1 x 10^6 cells/mL. The 5 µL Annexin V and 1 µL 100 µg/mL /propidium iodide working solution were added, incubated at room temperature for 15 min, and then 400 µL 1X Annexin-binding buffer was added and the mix kept on ice for immediate flow cytometry.

Quantification of reactive oxygen species

Reactive oxygen species (ROS) generation and quantification was with 2',7'-dichlorodihydrofluorescein diacetate (DCFDA)/H2DCFDA (dichlorofluorescein diacetate)-Cellular ROS Assay Kit (Abcam, ab113851) and 50 µM tert-butyl hydrogen peroxide was used as positive control per manufacturer's instructions. In brief, PD-L1^{KO} ID8agg cells were treated with vehicle control or chlorambucil (2.5 µM) for 48 hours, and then live cells were harvested and incubated with 20 µM H2DCFDA for 30 min at 37°C. Samples were analyzed by flow cytometry immediately with excitation and emission spectra of 485 and 535 nm, respectively.

Tumor initiating cell assessment

B16, ID8agg and ES2 cells were cultured 48 hours after reaching around 80% confluency, trypsinized using trypsin-EDTA (0.05%, GIBCO, Thermo Fisher, Waltham, Massachusetts, USA) and counted on a Vi-Cell (Beckman Coulter, Brea, California, USA). 2×10^6 B16 or ID8agg cells were stained with live dead viability dye (BioLegend), following by staining for tumor initiating cell (TIC) markers as previously described.[17 18] Briefly, B16 TICs were CD44$^+$CD133$^+$CD24$^+$ and ID8agg TIC were CD44$^+$CD24$^+$. In vivo TIC gating was done on tumor cells on the basis on their side and forward scatter, followed by gating for live, CD45$^-$CD44$^+$CD24$^+$ for ID8agg tumors. ALDEFLUOR kits were purchased from STEMCELL Technologies and used with 2×10^6 ES2 cells/ml. A 5 µL of the specific aldehyde dehydrogenase (ALDH) inhibitor diethylaminobenzaldehyde was added to control cells, incubated with 5 µL 4,4-difluoro-1,3,5,7,8-pentamethyl-4 -bora-3a,4a-diaza-*s*-indacene (BODIPY) amino acetaldehyde, a fluorescent substrate for ALDH and incubated for 45 min at 37°C, and kept in cold (4°C) PBS for remaining staining. N, N-diethylaminobenzaldehyde inhibits ALDH activity and was used as a positive control. ES2 TICs were defined as ALDH^{hi} by flow cytometry.

Western blotting and immunoprecipitation

To prepare whole cell lysates, cells were harvested and lysed in radioimmunoprecipitation assay buffer plus 1 mM phenylmethylsulphonyl fluoride and Halt protease/phosphatase inhibitor cocktail (Thermo Scientific) at 4°C. Protein concentrations were measured by BCA Protein Assay Kit (Thermo Scientific). Samples were run on precast 4%–15% sodium dodecyl sulfate polyacrylamide gels (Bio-Rad), transferred to polyvinylidene fluoride membranes (GE Water and Process Technologies) and blocked in 5% nonfat milk for 1 hour at ambient temperature. Membranes were then incubated with 1:1000 diluted primary antibodies against indicated proteins: αP70S6K (CST, cat. 34475), αp-P70S6K(Thr389) (CST, cat. 97596), α4EBP1(CST, cat.9644), αp-4EBP1(Ser65) (CST, cat. 9451), αRaptor (CST, cat. 48648), αLC3A/B (CST, cat. 4108), αPDL1 (CST, cat. 13684), αPDL1(Abcam, cat. 213480), αβ-TRCP (CST, cat. 4394), α GSK-3β (CST, cat. 12456), αPGSK-3β (CST, cat. 5558), αCBL-B (SC, cat. 376409), αVinculin (CST, cat. 13901). Cells for (co) immunoprecipitation experiments were seeded in 15 cm^2 dishes and cultured as described, using 6 million cells/immunoprecipitation reaction. For protein ubiquitination, cells were lysed in denaturing buffer (50 mM Tris-HCl, 0.5 mM EDTA and 1% SDS) followed by heating at 95°C for 10 min and then quenched with 9 volumes quenching buffer (0.5% Triton X-100, 20 mM Tris-HCl (pH 8.0), 137 mM NaCl, 10% glycerol, 2 mM EDTA). Protease inhibitor cocktail (Roche) was added fresh to all buffers. Cell lysates were incubated on a rotator for 30 min at 4°C, and then centrifuged at 20 000 × gravity for 15 min at 4°C. Supernatants were subsequently incubated with αPDL1 antibody overnight and processed using Dyna beads Protein G for immunoprecipitation (Thermo Fisher Scientific). The final eluate was processed, and Western blotting was performed with specific antibody binding detected by chemiluminescence using Western Lightening Plus regent (Perkin Elmer).

Quantitative real-time reverse transcription PCR

Total RNA was isolated from homogenized whole lung tissue with Trizol reagent (Invitrogen, cat. 15596026) according to manufacturer instructions. Subsequently, cDNA was synthesized with 1–2 µg of total RNA using the SuperScript III reverse transcriptase (Invitrogen, cat. 18080044). Quantitative PCR was conducted using the Bio-Rad Real-Time PCR System (Applied Biosystems), amplified with transcript-specific primers with SYBR Green (Thermo Scientific, cat. 4472908), according to manufacturer instructions. Mouse primers were: Tyr, 5′-CTCTGGGCTTAGCAGTAGGC-3′ and 5′- GCAAGCTGTGGTAGTCGTCT-3′; gp100, 5′-ACATTTCA TCACCAGCAGGGTGCC-3′ and 5′-AACAAGTGGGTGCT-GGCC-3′; Trp-2, 5′-GTCCTCCACTCTTTTACAGACG-3′ and 5′-ATTCGGTTGTGACCAATGGGT; Trp-1, 5′ CCCC TAGCCTATATCTCCCTTTT-3′ and 5′-TACCATCGTGGG GATAATGGC-3′; PDL1, 5′- GGTGGTGCGGACTACAAG-3′ and 5′- AACCCTCGGCCTGACATA-3′; and GPDH, 5′-AACGACCCCTTCATTGAC-3′ and 5′-TCCACGACATACT-CAGCAC-3′ as the internal control. Human primers PDL1, 5'-GCTTTTCAATGTGACCAGCA-3' and 5'- ATTTGGAG-GATGTGCCAGAG–3'; GAPDH, 5'-CGAGATCCCTC-CAAAATCAA-3' and 5'-TTCACACCCATGACGAACAT-3'.

Data were normalized to the endogenous reference gene GAPDH levels by the comparative CT (ΔΔCt) method.

Statistics

We used Prism software from GraphPad for statistical analyses. In bar graphs, data are shown as mean±SEM. We used two-way analysis of variance (ANOVA) corrected with Tukey post-tests to compare repeated means in tumor growth analyses. We used the log-rank test to analyze mouse survival from survival plots generated with the method of Kaplan-Meier. Three or more means were compared with one-way ANOVA with Tukey post-test. For comparison of two means, we used an unpaired t-test or Mann-Whitney U test. All analyses were considered $p<0.05$ as statistically significant.

RESULTS

Chlorambucil reduces tumor cell PDL1 in vitro and vivo

We performed high-throughput drug screens of the LOPAC and Prestwick Libraries (online supplemental figure S1A,B) to identify novel PDL1 depleting drugs for rapid clinical translation. As the screen used mouse melanoma cells, but we also wished to define PDL1 depletion agents in human cancer cells, 15 candidate drugs from the screen were verified for PDL1 depletion in ovarian cancer cells by flow cytometry. Chlorambucil and PMEG were among top hits (figure 1A and online supplemental figure S1C). Chlorambucil reduced surface PDL1 expression by 5-fold, which was greater than PMEG-mediated PDL1 reduction. We elected to study chlorambucil in detail as it is also FDA approved and orally bioavailable, whereas PMEG is not FDA approved. To validate flow cytometry data, we used immunoblots to detect total PDL1 in various human and mouse tumor cell lines, confirming chlorambucil as a bona fide tumor PDL1 depletion drug in all cell lines tested (figure 1B).

We further confirmed tumor PDL1 depletion by chlorambucil in vivo in a mouse ovarian cancer model. Chlorambucil significantly reduced the prevalence and mean fluorescence intensity of $PDL1^+$ cells among $CD45^-CD31^-FAP^-$ cells which are highly enriched for tumor cells, ersus control-treated mice (figure 1C, top panel and figure 1D). By contrast, PDL1 expression and prevalence in tumor fibroblasts and endothelial cells ($CD45^-CD31^+FAP^+$) and the $CD45^+$ immune cells were unchanged versus control-treated mice (figure 1C, bottom panel, figure 1E). Together, these data are consistent with tumor cell-selective PDL1 reduction by chlorambucil in vivo. Chlorambucil also reduced PDL1 expression in B16 tumor cells in vivo, but to a lesser degree versus in ID8agg (online supplemental figure S1D), possibly due to not excluding fibroblasts and endothelial cells in these analyses.

Chlorambucil inhibits tumor cell growth in vitro in a PDL1-dependent manner

Chlorambucil inhibited control B16 and ID8agg cell growth in vitro with no, or minimal killing or apoptosis induction (figure 2A), consistent with our previous findings of tumor intrinsic PDL1 promoting cell growth.[7] To determine if chlorambucil growth inhibitory inhibition was tumor cell PDL1-dependent, we tested genetic $PDL1^{KO}$ ES2, ID8agg and B16, all of which were less sensitive to chlorambucil-induced growth inhibition versus parental cells figure 2B, consistent with a tumor cell PDL1-dependent growth inhibition mechanism.

Chlorambucil is a DNA-damaging agent and DNA damage usually increases cell PDL1 expression.[19] To test the possibility that chlorambucil-mediated PDL1 reduction is not through its DNA-damaging effect, we first confirmed that chlorambucil at concentrations and in cells used here induced DNA damage (online supplemental figure S2A). We then tested other DNA-damage agents including X-rays, gemcitabine and the small molecule Chk1 inhibitor, rabusertib but none of these DNA damaging agents reduced tumor PDL1, but rather all increased it as expected (online supplemental figure S2B), suggesting that chlorambucil over-rides a normal biological response to DNA damage and that its PDL1 reduction effect is independent of its FDA-approved mechanism of action.

Chlorambucil inhibits tumor growth in vivo in a PDL1-dependent manner

We challenged WT mice orthotopically with poorly immunogenic and highly aggressive ID8agg cells, as we described[15] and treated with 2 mg/kg chlorambucil, which significantly reduced tumor growth and prolonged mouse survival versus PBS vehicle control (figure 3A,B). A 2 mg/kg chlorambucil also significantly improved survival in ID8agg challenged immunodeficient NSG mice versus vehicle control (figure 3C) demonstrating an immune-independent tumor growth control mechanism. By striking contrast, this same chlorambucil dose had no effect on the growth of orthotopic $PDL1^{lo}$ ID8agg tumors in WT mice as detected by ascites weight gain and end-experiment tumor weights (figure 3D, online supplemental figure S3A) suggesting that the chlorambucil efficacy mechanism in this model is tumor PDL1-dependent and immune-independent. To test chlorambucil in a distinct tumor model and different anatomic compartment, B16 melanoma cells were challenged subcutaneously into WT or NSG mice. Similar to peritoneal ID8agg ovarian cancer, 3 mg/kg chlorambucil significantly inhibited tumor growth and prolonged mice survival in WT mice and NSG mice, but less effectively in NSG mice (figure 3E,F). In contrast to $PDL1^{lo}$ ID8agg, this chlorambucil dose also inhibited $PDL1^{KO}$ B16 tumor growth in WT mice (figure 3G), although significantly less effectively than in control B16 (figure 3H). In NSG mice, chlorambucil efficacy against $PDL1^{KO}$ B16 tumor was abolished (figure 3I), again demonstrating a PDL1-dependent treatment mechanism, but in this case it was also immune-dependent in striking contrast to ID8agg. Thus, chlorambucil treatment efficacy is tumor PDL1-dependent, but at selected chlorambucil doses or in

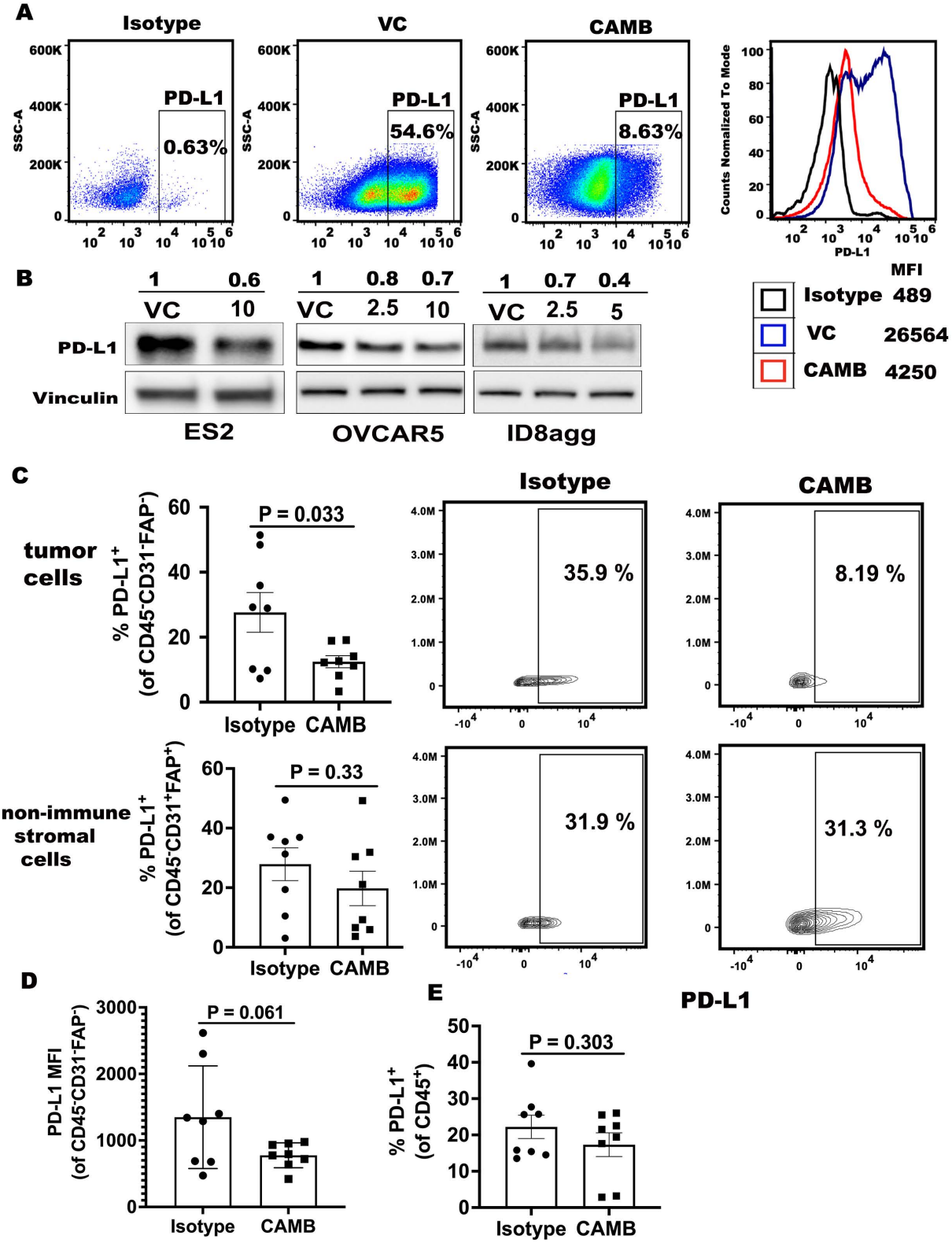

Figure 1 Chlorambucil reduces tumor PDL1 in vitro and in vivo. (A) Flow cytometry for PDL1 percentage and mean fluorescence intensity (MFI) in VC (vehicle control) and chlorambucil treatment (10 µM, 48 hours) in OVCAR5 cells in vitro. (B) Western blots for PDL1 expression in human and mouse ovarian cancer cells treated in vitro with (+) or without (–) chlorambucil for 48 hours. Vinculin, loading control. Values are µM chlorambucil. (C) Flow cytometry analyses of WT mice challenged with ID8agg cells, treated with chlorambucil (CAMB, 1 mg/kg as described in methods) and sacrificed 4 weeks post tumor challenge. Summary of PDL1 percentage in the tumor $CD45^-CD31^-FAP^-$ (top) or non-immune stromal cell $CD45^-CD31^+FAP^+$ (bottom) gates. PDL1 percentage in specified populations as indicated (right). (D) Summary graph of PDL1 MFI in $CD45^-CD31^-FAP^-$ tumor cells. (E) Summary of PDL1 percentage in $CD45^+$ immune cells. P value determined by unpaired t-test. VC, vehicle control.

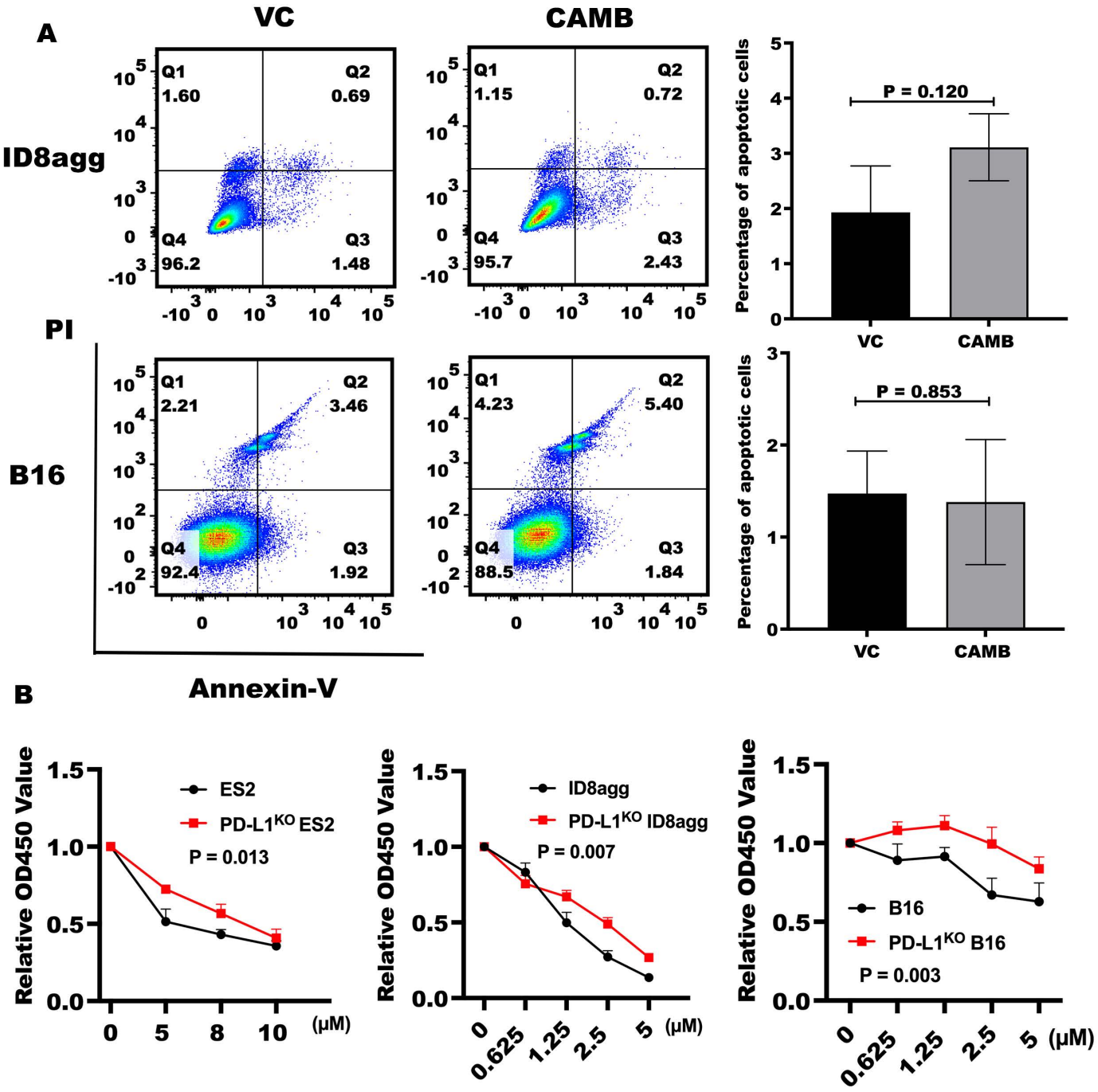

Figure 2 Chlorambucil slows tumor cell growth in a tumor PDL1-dependent fashion. (A) Annexin V-FITC/propidium iodide (PI) staining by flow cytometry. In given plots: Q1, necrotic cells, Q2, late apoptotic cells, Q3, live cells and Q4, early apoptotic cells. ID8agg (upper panel) and B16 cells (lower panel) were treated with 2.5 µM chlorambucil for 48 hours. Numbers in each quadrant indicate percent cells. Summary and stats for total (early+late) apoptotic cells shown on the right. (B) Tumor cells were treated with indicated concentrations of chlorambucil for 48 hours. Cell viability was detected by CCK-8 assay and relative cell viability ratios were compared between control cells and genetically PDL1-depleted cells. Data represents three independent experiments. P value determined by unpaired t-test. VC, vehicle control.

specific tumors, treatment efficacy could be dependent or independent of immune contributions.

To test whether chlorambucil efficacy is host PDL1 dependent, we challenged ID8agg cells or B16 cells into PDL1^{KO} mice. In both cases, chlorambucil efficacy was unaffected (figure 3J,K; online supplemental figure S3B). Thus, chlorambucil-mediated tumor growth inhibition depends on tumor rather than host PDL1, also consistent with its tumor cell-selective PDL1 depletion that is neither cancer nor anatomic compartment-specific in these models.

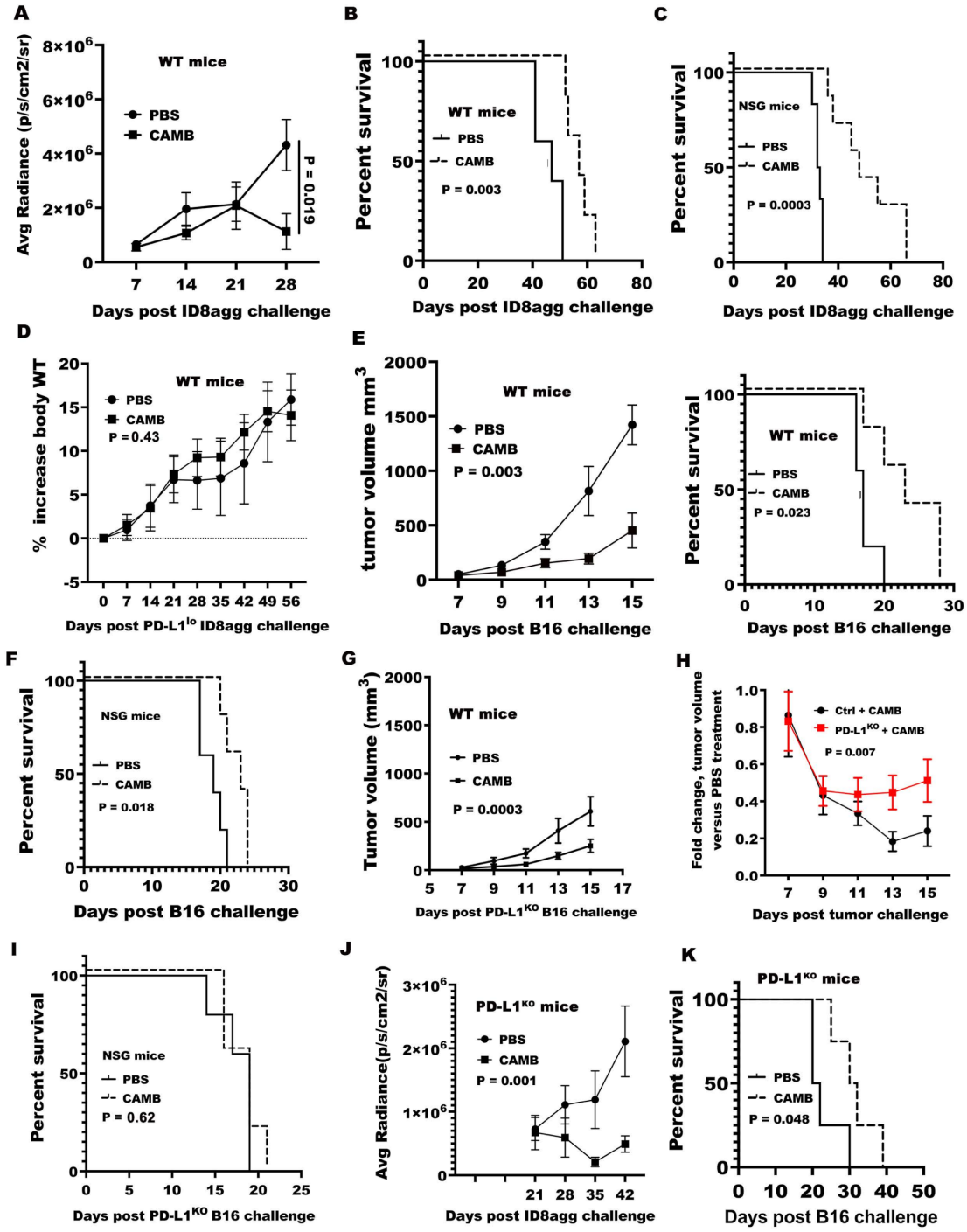

Figure 3 Chlorambucil treats tumors in vivo in a tumor PDL1-dependent fashion. (A) ID8agg-luc tumor bioluminescence was measured in WT mice treated with chlorambucil (2 mg/kg) as described. N=5/group. P value, two-way ANOVA. (B, C) Kaplan-Maier survival curve in WT (B) or NSG mice (C) treated with chlorambucil 2 mg/kg as described. P value from log-rank test. N=5/group in WT mice and 6/group in NSG mice. (D) WT mice challenged with PDL1^{lo} ID8agg cells and treated as described in (A). Mice body weight measured weekly and increase is relative to baseline. N=5 for PBS and six for chlorambucil, p value, two-way ANOVA. (E) Tumor growth of WT mice challenged with B16 cells and treated with 3 mg/kg chlorambucil, with the last treatment on day 18, N=5 for all groups. P value, two-way ANOVA. Kaplan-Maier survival curve in these WT mice (right panel). (F) Kaplan-Maier survival plot of NSG mice (N=5/group) challenged with B16 cells and treated with 3 mg/kg chlorambucil. (G) Tumor growth in WT mice challenged with PDL1^{KO} B16 cells and treated with 3 mg/kg chlorambucil. N=5/group. (H) Tumor growth fold-change calculated as control treatment divided by chlorambucil treatment calculated separately for control and PDL1^{KO} tumors on the given days shown. P value, χ^2 test. (I) Kaplan-Maier survival curve of NSG mice challenged with PDL1^{KO} B16 cells and treated with chlorambucil as in (G). N=5/group. (J) Tumor bioluminescence of PDL1^{KO} mice challenged with ID8agg-luc cells and treated as in (A). N=6/group. P value, two-way ANOVA. (K) Kaplan-Maier survival curve of PDL1^{KO} mice challenged with B16 cells and treated as described in (E). N=4 for both PBS and CAMB. ANOVA, analysis of variance; CAMB, chlorambucil; PBS, phosphate-buffered saline.

Chlorambucil renders αPDL1-refractory tumors αPDL1-responsive

We reported that αPDL1 is ineffective against control intraperitoneal ID8agg[15] and subcutaneous PDL1^{KO} B16 tumor[7] challenged in WT mice. As sufficient chlorambucil can inhibit PDL1^{KO} B16 tumor growth with evidence for immune contributions, we tested if a lower chlorambucil dose that was ineffective as a single agent would improve αPDL1 efficacy. Cutting the chlorambucil by 50% to 1.5 mg/kg rendered it ineffective against PDL1^{KO} B16, but its combination with αPDL1 (also ineffective as a single agent) significantly inhibited PDL1^{KO} B16 tumor growth and improved survival in WT mice (figure 4A). Further, this combination inhibited spontaneous lung metastases following subcutaneous challenge compared with single-agent treatment as detected by qRT-PCR for melanoma specific gene products (figure 4B). Cutting the chlorambucil by 50% to 1 mg/kg failed to inhibit control ID8agg tumor growth but greatly sensitized it to αPDL1 growth inhibition and significantly prolonged WT mice survival (figure 4C,D). Although chlorambucil alone did not treat PDL1^{lo} ID8agg (figure 3D) adding αPDL1 significantly improved survival of WT mice challenged with PDL1^{lo} ID8agg versus chlorambucil alone, including apparent tumor cure in 3 of 6 mice, vs 0 of 6 cures in control treated WT (right panel, figure 4E). The foregoing all together suggested that chlorambucil could elicit tumor PDL1-independent immunogenicity as a mechanism to improve αPDL1 outcomes especially in PDL1 depleted tumors in which αPDL1 alone is ineffective.

Immunogenic cell death that can stimulate anticancer immunity and treatment efficacy is elicited by certain cytotoxic agents,[20–22] although chlorambucil is not reported to be a major immunogenic cell death inducer. However, we found that cell surface calreticulin, a measure of immunogenic cell death, was PDL1-dependently increased by chlorambucil in ID8agg but not B16 cells, although maximal immunogenic cell death was equivalent in control or genetically PDL1 depleted cells in both cell lines (figure 4F, online supplemental figure S4A). To assess if lower chlorambucil could define an ICD difference in B16 vs PD-L1^{KO} B16 we tested chlorambucil concentrations down to 0.625 µM but without any PDL1-dependent effect (online supplemental figure S4B). Reactive oxygen species can evoke immunogenic cell death,[23] but were barely detectable in control and PDL1^{KO} cells although they were robustly elicited by hydrogen peroxide positive control (online supplemental figure S5A). Thus, chlorambucil-induced immunogenic cell death is a candidate mechanism for improving αPDL1 efficacy in some tumor models, but not others, which requires further investigations.

αPDL1 improves immunity in combination with chlorambucil

To understand immune effects of chlorambucil contributing to αPDL1 efficacy, we evaluated the immune landscape in ascites and tumors from different treatment groups of ID8agg-challenged mice. T-distributed stochastic neighbor embedding analysis of flow cytometry data demonstrated pronounced differences in tumor immune landscapes among treatment groups (online supplemental figure S6A). Chlorambucil alone did not appreciably alter antitumor immune cells known to mediate antitumor immunity, consistent with its immune-independent mode of action in this tumor. Combination treatment with αPDL1 did not significantly increase CD8$^+$ T cell numbers nor their production of IFN-γ$^+$ or Granzyme B$^+$ (online supplemental figure S6B). However, chlorambucil plus αPDL1 additively increased CD44$^+$CD62L$^+$ central memory CD8$^+$ T cells and a population of CD8$^+$ CXCR5$^+$TCF1$^+$ CCR2$^+$ T cell stem cells that can contribute to ICB response[24] in ID8agg (figure 5A).

In contrast to CD8$^+$ T cell data, an NK1.1$^+$ cell cluster (P2) in ID8agg-bearing mice was increased only after combination chlorambucil plus αPDL1 treatment (online supplemental figure S6A), which also increased NK cell granzyme B, an important antitumor effector molecule, versus chlorambucil alone (figure 5B), suggesting NK cells could contribute to combination treatment efficacy in ID8agg. To test functional memory after combination chlorambucil and αPDL1 treatment, we could only study PDL1^{lo} ID8agg as there were no cures in ID8agg mice. We rechallenged three mice cured of ID8agg by chlorambucil, showing a trend to tumor protection that did not reach statistical significance (figure 5C) possibly due to low numbers of available cured mice.

We next analyzed immune outcomes in PDL1^{KO} B16 challenge in WT mice, in which chlorambucil alone exerts immune-dependent treatment effects, after combination treatment. In PDL1^{KO} B16 tumors, chlorambucil significantly increased total NK cells but not CD8$^+$ T cells, although adding αPDL1 did not augment either of these cell populations (online supplemental figure S6C,D). We did, however, note a significant reduction in exhausted PD1$^+$ NK cells but only in combination treated PDL1^{KO} B16 tumors (figure 5D) further suggesting the involvement of NK cells in combination treatment efficacy and we found terminally exhausted CD8$^+$ T cells expressing both PD1 and Tim3 only in combination treated PDL1^{KO} B16 tumors (figure 5E), suggesting that NK cells improve antitumor T cell functions in this tumor. To test a functional role for NK cells in mediating the antitumor effect of chlorambucil plus aPDL1 combination therapy, we depleted NK cells during combination treatment (online supplemental figure S7A), which completely abolished combination treatment efficacy in ID8agg challenge (figure 5F). These results confirm an essential role for NK cells in mediating the efficacy of this combination.

We also considered that NK cell contributions to single-agent chlorambucil treatment efficacy are unreported. As chlorambucil efficacy in PDL1^{KO} B16 tumor as a single agent is immune-dependent (figure 3I), we studied NK cells in PDL1^{KO} B16 tumor by challenging PDL1^{KO} B16 cells into WT mice, treated with chlorambucil and used α-NK1.1 to deplete NK cells, which totally abolished chlorambucil efficacy as seen in reduced tumor growth control

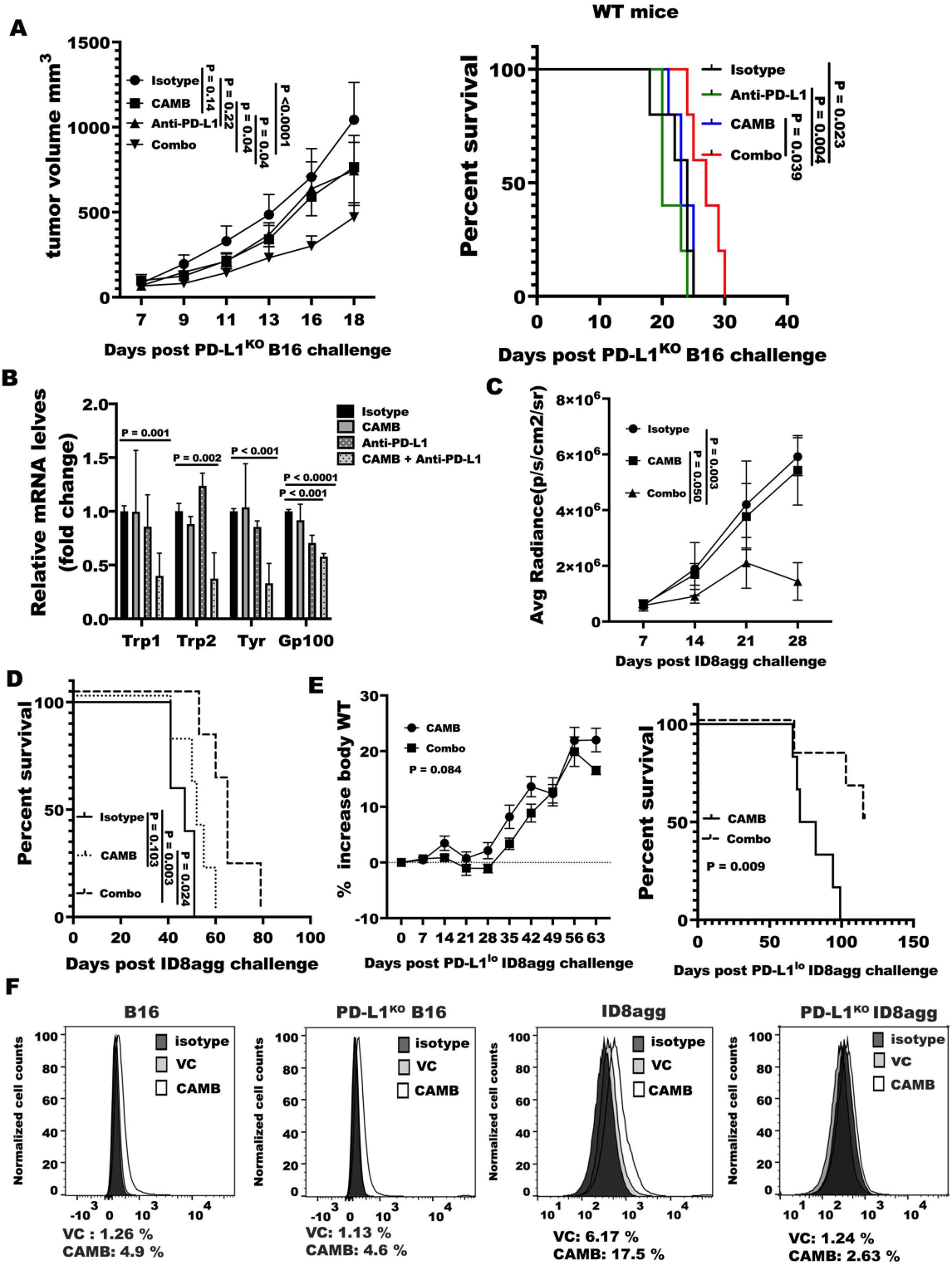

Figure 4 Chlorambucil improves αPDL1 treatment efficacy in vivo. (A) Tumor growth (left) and survival (right) of WT mice (N=5/group) challenged with PDL1^{KO} B16 and treated with 1.5 mg/kg chlorambucil±anti-PDL1 100 µg/mouse (combination is chlorambucil plus anti-PDL1). (B) qRT-PCR for indicated melanoma specific genes in whole lung tissue harvested on day 20 after tumor challenge with PDL1^{KO} B16 cells into WT mice and treated as in panel A. P value, unpaired t-test. (C, D) ID8agg-luc tumor bioluminescence (C) and survival (D) in WT mice (N=5–6/group) after treatment with 1 mg/kg chlorambucil as described, ±a 100 µg/mouse nti-PDL1on days 7, 11, 15 and 19. P value, two-way ANOVA. (E) Body weight gain (as surrogate measurement for tumor burden) (left) and survival (right) of WT mice (N=6/group) challenged with PDL1^{lo} ID8agg and treated with 2 mg/kg chlorambucil±anti-PDL1 as in panel D. P value, two-way ANOVA. (F) Flow cytometry analysis of calreticulin content in vehicle control (VC) or chlorambucil (CAMB)-treated B16 or PDL1^{KO} B16 (1.25 µM), ID8agg or PDL1^{KO} ID8agg (1.25 µM), for 48 hours. Isotype: isotype control for anti-calreticulin antibody. Figures below panels, % positive cells. Data represent one of three independent experiments with similar results. ANOVA, analysis of variance.

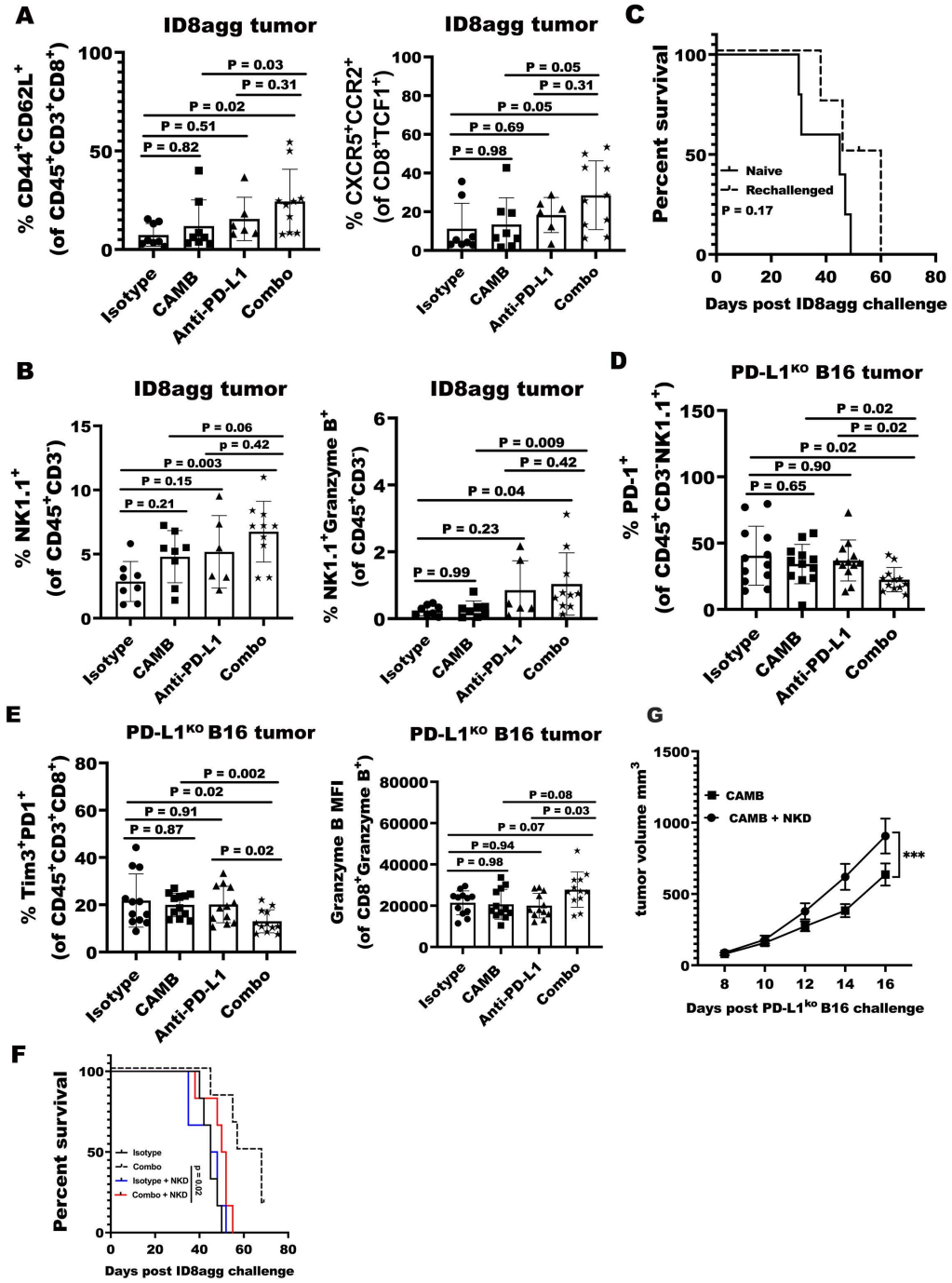

Figure 5 αPDL1 improves CAMB-mediated immunity. (A) Summary statistics for flow cytometry data for $CD8^+CD44^+CD62L^+$ effector memory (left) and $CD8^+CXCR5^+TCF1^+CCR2^+$ T cell stem cell abundance from mice ascites which challenged with ID8agg and treated with chlorambucil±anti-PDL1 or isotype as a control. Mice are sacrificed after tumor challenged 30 days, P value, one-way ANOVA, chlorambucil vs combination and anti-PDL1 vs combination using Mann-Whitney test. (B) Flow cytometric analysis of NK cell frequency and Granzyme B production in $CD45^+CD3^-NK1.1^+$ NK cells in ascites after challenge with ID8agg cells and treatment with chlorambucil±anti-PDL1 treatment as described. P value, one-way ANOVA. Chlorambucil versus combination and anti-PDL1 versus combination P value by Mann-Whitney U test. (C) Mice previously cured of $PDL1^{lo}$ ID8agg challenge by combination treatment from figure 4E (N=3) were rechallenged with ID8agg cells 105 days after final treatment. 'Naïve mice' (N=5) were controls not previously challenged or treated. Kaplan-Maier plot of survival shown. (D, E) Flow cytometric analysis of $PDL1^{KO}$ tumor from WT mice challenged orthotopically with $PDL1^{KO}$ B16 cells and treated as described. (D) $PD1^+$ (exhausted) $CD45^+CD3^-NK1.1^+$ NK cells. E. $PD1^+Tim3^+$ (exhausted) $CD8^+$ T cells. P value, one-way ANOVA, chlorambucil versus combination and anti-PDL1 vs combination by Mann-Whitney test. (F) Kaplan-Maier survival plot of WT mice challenged with ID8agg cells (N=6/group) treated with chlorambucil+anti-PDL1 combination as described in figure 4C ±Anti-NK1.1 antibody or isotype control (250 µg/mouse) on days 6, 10, 14, 18, 22, 26. (G) $PDL1^{KO}$ B16 cells challenged into WT mice and treated with chlorambucil as described ± α-NK1.1 to deplete NK cells. N=10 tumors/group. P value, unpaired t-test. ANOVA, analysis of variance; CAMB, chlorambucil; NK, natural killer.

(figure 5G) and end-experiment tumor weight (online supplemental figure 8A). NK cell depletion generated more terminally exhausted $CD8^+$ T cells expressing both PD1 and Tim3 with less Granzyme B production (online supplemental figure 8B,C) consistent with data in combination treatment, and with improved antitumor T cell function as a candidate downstream efficacy mechanism of chlorambucil-activated NK cells.

Chlorambucil promotes PDL1 degradation through the ubiquitin-proteasome pathway

To understand how chlorambucil reduced tumor PDL1 content we first assessed transcription of *CD274*, the gene encoding PDL1. *CD274* mRNA in human OVCAR5 ovarian cancer cells was slightly increased by chlorambucil treatment whereas *CD274* mRNA in ID8agg cells was significantly reduced (figure 6A). These data suggested that chlorambucil-mediated PDL1 depletion mechanisms include transcriptional control in mouse ID8agg cells, but that mechanisms could differ in human versus mouse cells or could differ due to underlying mutational differences in distinct tumors (eg, OVCAR5 in KRAS mutated[25] whereas ID8agg is KRAS WT[26]). A recent report showed that homeostatic PDL1 regulation includes its degradation through ubiquitination.[27] We treated OVCAR5 cells with MG132, a proteasome inhibitor, which increased PDL1 expression and abolished chlorambucil-mediated PDL1 reduction (figure 6B) suggesting ubiquitin-mediated PDL1 degradation as a mechanism of chlorambucil reducing PDL1 level in these cells. To evaluate PDL1 ubiquitination further after chlorambucil treatment, a co-immunoprecipitation assay was performed, showing that ubiquitinated PDL1 in OVCAR5 and human ovarian cancer ES2 cells was increased after chlorambucil treatment (figure 6C, online supplemental figure S9A), supporting the concept that chlorambucil promotes PDL1 degradation through the ubiquitin-proteasome pathway. E3 ligases play an important role in PDL1 degradation signaling.[28 29] β-TRCP and CBL-B are two E3 ligases mediating PDL1 degradation.[30 31] We used siRNA against E3 ligase β-TRCP and it blocked PDL1 degradation by chlorambucil in OVCAR5 cells, whereas knock down of the CBL-B E3 ligase did not (figure 6D; online supplemental figure S9B,C), suggesting chlorambucil works through β-TRCP to promote PDL1 ubiquitination. PDL1 can undergo GSK3β/β-TRCP mediated proteasomal degradation.[32] We found that GSK3β was activated as seen by reduced phosphorylation of GSK3β with chlorambucil treatment in OVCAR5 cells (figure 6E). Epidermal growth factor inhibits GSK3β activity and stabilizes PDL1.[32 33] Incubation of cells with recombinant epidermal growth factor to block the GSK3β pathway during chlorambucil exposure restored PDL1 expression (figure 6F). Together, these data show that chlorambucil promotes PDL1 degradation through GSK3β/β-TRCP-mediated ubiquitination in some ovarian cancer cell lines.

Chlorambucil phenocopies genetic PDL1 depletion on mTORC1, autophagy and TIC numbers in vitro

To explore the translational potential of chlorambucil as a PDL1 depleting drug further, we tested if it affected pathways reported from genetic $PDL1^{KO}$ studies. Western blots showed that chlorambucil inhibits mTORC1 signaling as assessed by p-$P70S6K^{T389}$ and p-$4EBP1^{S65}$ and increased LC3 lipidation indicative of increased autophagic flux (figure 7A,B), consistent with our published data that tumor cell-intrinsic PDL1 promotes mTORC1 and suppresses autophagy, including in ovarian cancer cells.[7] As we also reported that tumor intracellular PDL1 promotes TIC generation,[34] we evaluated TIC content in ES2, ID8agg and B16 cells by flow cytometry using well-accepted TIC markers for each. Chlorambucil significantly reduced $ALDH^{hi}$ TICs in ES2 cells (figure 7C, upper panel) and $CD44^+CD24^+$ and $CD44^+CD133^+CD24^+$ TIC populations in B16 and ID8agg cells, respectively (figure 7C, lower panel). In vivo, TICs from ID8agg tumor tissue were also reduced by lower dose chlorambucil (figure 7D). Thus, pharmacological PDL1 depletion with chlorambucil phenocopies other important genetic tumor PDL1 knockout effects, which could also be exploited therapeutically.

DISCUSSION

Pathological signals from surface-expressed tumor or immune cell PDL1 can be mitigated by αPDL1 ICB antibodies, but most patients still do not benefit from such treatment. Whereas many immune and treatment outcomes from surface-expressed tumor PDL1 are described, PDL1 also generates significant tumor cell-intrinsic signals. For example, recent findings that cell-intrinsic tumor PDL1 signals mediate treatment resistance signals including to targeted small molecules, cytotoxic drugs, irradiation and αPD1 ICB immunotherapy suggest new insights into tumor immunopathogenesis and opportunities for novel treatment approaches. The subject of tumor-intrinsic PDL1 signals was recently comprehensively reviewed.[35]

Almost all studies of tumor-intrinsic PDL1 signals use scientifically rigorous genetic PDL1 depletion to establish proofs-of-concept that depleting tumor-intrinsic PDL1 and/or its downstream tumor signal consequences can reduce treatment resistance, slow growth or reduce metastatic spread among other clinical benefits.[35] Nonetheless, genetic PDL1 depletion is not presently clinically practical, leading to investigations of pharmacological means to reduce tumor-intrinsic PDL1 signals. For example, the benzoporphyrin verteporfin that is FDA-approved to treat retinal diseases reduces the content of PDL1 in different human cancer lines, but not tumor-selectively. It augments treatment efficacy of a poly (ADP-ribose) polymerase inhibitor in vivo in mouse models of ovarian cancer.[36] Curcumin is a natural product that reduces content of cancer cell PDL1 through ubiquitination in mouse 4T1 breast cancer cells and augmented efficacy of

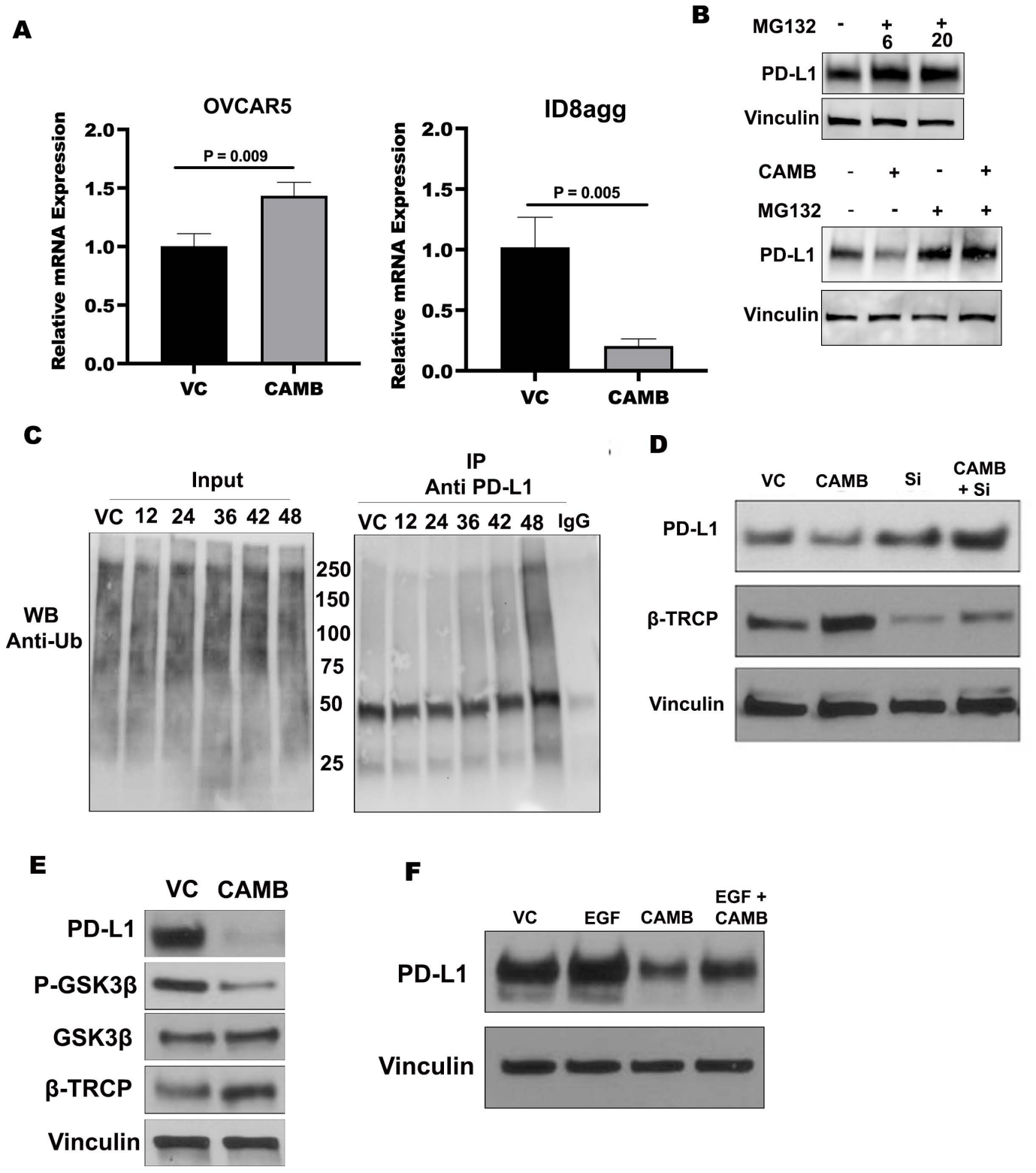

Figure 6 CAMB reduces PDL1 through GSK3β/β-TrCP ubiquitination promotion. (A) RT-qPCR for *CD274* mRNA in OVCAR5 and ID8agg cells treated with (+) or without (–) chlorambucil (10 µM for OVCAR5 and 2.5 µM for ID8agg) for 48 hours. (n=4). (B) Western blot for PDL1 protein in OVCAR5 cells with (+) or without (–) MG132 (2 µM) for 6 or 20 hours (upper panel). PDL1 expression in OVCAR5 cells treated with chlorambucil (2.5 µM) 48 hours with or without MG132 (2 µM) in the final 6 hours (lower panel). (C) OVCAR5 cells treated with chlorambucil for indicated times (hours) and then PDL1 was immunoprecipitated (IP) using anti-PDL1 (1:50) antibody and subjected to Western blot analysis with anti-ubiquitin (Ub) antibody. Molecular weights shown to left of IP blot. (D) Western blot for PDL1 after 48-hour incubation of OVCAR5 cells with chlorambucil (2.5 µM) incubation, siRNA against β-TrCP (si) or both. (E) Western blot for GSK3β activation and β-TrCP in OVCAR5 cells after chlorambucil (2.5 µM, 48 hours) incubation. (F) Western blot for PDL1 with chlorambucil (2.5 µM) or epidermal growth factor (EGF) 30 ng/mL for 48 hours in OVCAR5 cells. CAMB, chlorambucil; VC, vehicle control.

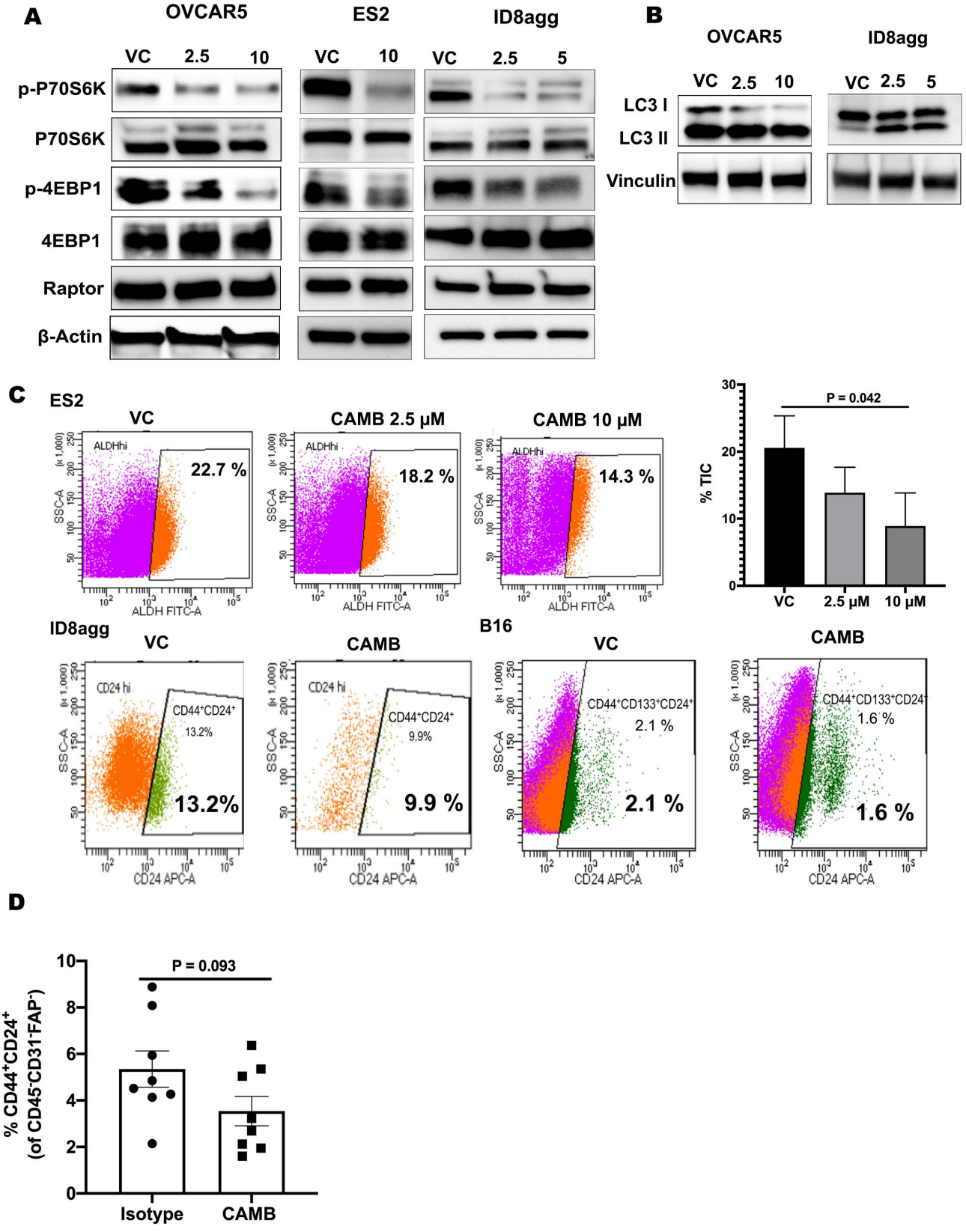

Figure 7 CAMB suppresses mTORC1, augments autophagy and reduces TIC numbers. (A) Western blots for mTORC1 pathway proteins in OVCAR5, ES2 and ID8agg cells treated with chlorambucil (μM dose indicated) for 48 hours. (B) Western blot for LC3I/II to assess autophagy in cell lysates treated±chlorambucil (μM dose) at indicated concentrations. (C) Percent ALDH^{hi} TIC by flow cytometry in ES2 cells cultured±chlorambucil. Percent CD44^{+}CD24^{+} ID8agg TIC and CD44^{+}CD133^{+}CD24^{+} B16 TIC with chlorambucil 2.5 μM treated with 48 hours detected by flow cytometry. Summary statistics graph for each cell line shown. (D) Summary graph of TIC number in ID8agg tumors assessed by flow cytometry after treatment with chlorambucil (1 mg/kg) from day 7 to day 28 as described above. CAMB, chlorambucil; VC, vehicle control.

immunotherapy against 4T1 with anti-CTLA4 in vivo.[37] Oxymatrine is a quinolizidine alkaloid natural product that reduces PDL1 content in human colorectal cancer lines through epigenetic control and is cytotoxic to these cell lines in vitro.[38]

To identify orally available pharmacological means to inhibit tumor intracellular PDL1 signals with ease of administration, we used a high throughput drug screen of two libraries enriched in FDA-approved agents or those in clinical trials that identified 15 FDA-approved drugs and 2 non-FDA-approved molecules that are candidate tumor PDL1 depletion agents. We validated chlorambucil and PMEG as *bona fide* tumor PDL1 depleting drugs, and then focused on chlorambucil as it is orally bioavailable whereas PMEG is not, relatively safe and tolerable at low doses, relatively inexpensive, and FDA-approved. PMEG is also not FDA-approved. Thus, chlorambucil could be rapidly tested clinically.

Chlorambucil effectively reduced mouse and human ovarian cancer and melanoma cell PDL1 content in vitro. It relatively selectively depleted PDL1 from tumor but not stromal or local immune cells in vivo but further work is required to understand this relative selectively, which we speculate could owe at least in part to differences in post-translational modifications in PDL1 in tumor versus non-malignant cells.[39–41] Its treatment efficacy was tumor PDL1-dependent in vitro and in vivo and was host PDL1-independent in vivo, all consistent with relative tumor PDL1 selectivity. In support of pharmacological cell-selective PDL1 depletion as a treatment strategy, we previously reported that the small molecule PPAR-γ antagonist GW9662 selectively reduced adipocyte (but not tumor) PDL1 to improve αPDL1 immunotherapy efficacy against breast cancer in mouse models.[42] Thus, some drugs can be repurposed to deplete PDL1 in a cell-selective manner, although mechanisms for such cell selectivity remain obscure.

Chlorambucil efficacy here is notable in being improved by tumor PDL1, whereas tumor-intrinsic PDL1 signals generate resistance to most reported treatment approaches to date including cytotoxic chemotherapy, small molecules and irradiation.[6–9 43] Nonetheless, we reported that tumor PDL1 reduces mouse melanoma and ovarian cancer cell resistance to chloroquine in vitro and in vivo.[7] PDL1 sensitization to a targeted small molecule is also not a class effect as chloroquine is not chemically related to chlorambucil and has a distinct mechanism of action for its FDA-approved indication. Tumor PDL1 also sensitized $BRAF^{V600E}$ mutated colon cancer cells to cytotoxic chemotherapy in vitro and in vivo[44] although mechanisms were not defined. Chlorambucil-mediated PDL1 reduction is also notable in that most DNA damaging agents increase PDL1.[45 46]

Chlorambucil growth inhibition is not clearly from direct tumor cell cytotoxicity as proliferation inhibition in vitro was not due to significant cell death at concentrations tested, which are at or above those achievable in vivo. Whether this growth inhibitory effect relates to altered mTORC1, autophagy or TICs that we also showed to be elicited by chlorambucil-mediated PDL1 depletion, versus other factors, requires additional investigation. Although PD1 and CD80 are known PDL1 ligands, most reports of tumor cell-intrinsic signals for these outcomes are little reported and also merit further studies.

Notably, chlorambucil-mediated tumor growth inhibition was immune-independent in some settings, whereas host immunity contributed in others. At higher chlorambucil doses, efficacy was tumor PDL1-dependent but host immune independent, suggesting effects directly and exclusively on tumor. Our finding that lower doses improved αPDL1 efficacy in αPDL1-refractory ID8agg tumors are consistent with an immune effect which could relate to chlorambucil elicitation of immunogenic cell death that we demonstrated. As a DNA damaging agent it could also activate immunogenic STING signals known to improve ICB efficacy,[47] an area for further study.

Improvement of $PDL1^{KO}$ B16 response to αPDL1 suggests a PDL1-independent component of chlorambucil efficacy in some tumors, which also could include induced tumor immunogenicity. Our flow cytometry data suggested NK cell activation as a candidate mechanism for chlorambucil contributions to immune efficacy, supported by our NK cell depletion data, which reduced chlorambucil efficacy alone and in combination with αPDL1. Chlorambucil appears to activate NK cells that promote antitumor T cell immunity, an area requiring further investigations, but suggesting that combinations of chlorambucil with NK cell activating molecules could be a useful treatment strategy in selected cancers.

Adding chemotherapy to ICB has proven efficacious in various settings[48–50] and is FDA approved in small cell and non-small cell lung cancers and triple negative breast cancer using αPD1 or αPDL1 ICB. Chemotherapy is thought to improve tumor immunogenicity in this setting, which could be from vaccination from antigens or DNA exposed in dying cancer cells or immunogenic cell death among other considerations recently reviewed.[51] A case report showed that chlorambucil improved αPDL1 efficacy in chronic lymphocytic leukemia patient.[52] Thus, chlorambucil mediates multiple mechanisms for treatment efficacy in difficult-to-treat cancers including PDL1-dependent mechanisms we report here, such as inducing immunogenic cell death in selected cancers. Why some tumors are more susceptible to chlorambucil-mediated immunogenic cell death induction is an area for further investigation.

Chlorambucil-mediated tumor PDL1 reduction includes at least two distinct mechanisms that differ in distinct tumor types. A better understanding of its specific mechanisms of action in distinct tumor types could inform specific and perhaps better treatment combinations. Likewise, chlorambucil was not designed to deplete PDL1. Medicinal chemistry could improve this feature while reducing other undesirable functions. However, chlorambucil DNA damage induction could be useful to improve tumor immunogenicity to boost efficacy of various treatment approaches.

Further studies of intracellular tumor PDL1 signals, other approaches to their inhibition and additional tumor-PDL1 depletion drugs are warranted, a subject we just reviewed.[6] Finally, recent reports demonstrate effects of tumor-intrinsic PDL1 in specific subcellular locations such as nuclear PDL1 control of αPD1 efficacy,[11] pyroptosis[12] and genomic stability,[53 54] areas requiring further investigations.

Author affiliations
[1]Department of Medicine, University of Texas Health, San Antonio, Texas, USA
[2]Department of Medicine, University of Texas Health Science Center, San Antonio, Texas, USA
[3]Medicine, University of Texas Health, San Antonio, Texas, USA
[4]The Graduate School of Biomedical Sciences, UTHSCSA, San Antonio, Texas, USA
[5]Med Hematology/Oncology, UT Health Long School of Medicine, San Antonio, Texas, USA
[6]UT Health Long School of Medicine, San Antonio, Texas, USA
[7]Division of Hematology/Medical Oncology, UT Health Long School of Medicine, San Antonio, Texas, USA
[8]Department of Immunology, Duke School of Medicine, Durham, NC, USA
[9]Medicine, University of Texas Health Science Center, San Antonio, Texas, USA

Twitter Suresh J Kari @Kari1Suresh

Acknowledgements We thank The Center for Investigational Drug Development for conducting drug screening.

Contributors TC and HB developed and interpreted experiments. TC wrote and edited the manuscript and provided overall project guidance. HB performed experimental work and helped edit the manuscript. YD performed flow cytometry and interpreted flow cytometry data. ASP performed mouse experiments and charted data. YJL performed immunoblots and ROS detection. AK, CJM, MG, CO and RMR helped with mouse tissue processing for immune data acquisition and analyses. HBG assisted with TIC experiments. AVRK and SJK performed immunoblots. JRC-G provided intellectual input, advised on tumor models and cursed incompetent referees. TC in the guarantor responsible for overall and full responsibility.

Funding STARS (no number), Owens Foundation (no number), the UTHSA Daisy M. Skinner endowment (no number), Clayton Foundation (no number), The Dartmouth Gmelich endowment (no number), NIH (GM113896, TL1 TR002647, CA054174, CA205965, CA239390, AG021890 GM113896, TR002647).

Competing interests TC and ARK have filed a patent on PDL1 depletion drugs.

Patient consent for publication Not applicable.

Provenance and peer review Not commissioned; externally peer reviewed.

Data availability statement Data are available on reasonable request.

ORCID iDs
Aravind Kancharla http://orcid.org/0000-0001-9095-7735
Ryan Michael Reyes http://orcid.org/0000-0002-9562-5809
Harshita B Gupta http://orcid.org/0000-0003-1003-2658
Tyler Curiel http://orcid.org/0000-0001-6962-9411

REFERENCES

1 Hayashi H, Nakagawa K. Combination therapy with PD-1 or PD-L1 inhibitors for cancer. *Int J Clin Oncol* 2020;25:818–30.
2 Topalian SL, Taube JM, Pardoll DM. Neoadjuvant checkpoint blockade for cancer immunotherapy. *Science* 2020;367. doi:10.1126/science.aax0182. [Epub ahead of print: 31 Jan 2020].
3 Tang H, Liang Y, Anders RA, *et al*. PD-L1 on host cells is essential for PD-L1 blockade-mediated tumor regression. *J Clin Invest* 2018;128:580–8.
4 Rizvi NA, Cho BC, Reinmuth N, *et al*. Durvalumab with or without tremelimumab vs standard chemotherapy in first-line treatment of metastatic non-small cell lung cancer: the Mystic phase 3 randomized clinical trial. *JAMA Oncol* 2020;6:661–74.
5 Rajan A, Heery CR, Thomas A, *et al*. Efficacy and tolerability of anti-programmed death-ligand 1 (PD-L1) antibody (Avelumab) treatment in advanced thymoma. *J Immunother Cancer* 2019;7:269.
6 Kornepati AVR, Vadlamudi RK, Curiel TJ. Programmed death ligand 1 signals in cancer cells. *Nat Rev Cancer* 2022;22:174–89.
7 Clark CA, Gupta HB, Sareddy G, *et al*. Tumor-Intrinsic PD-L1 signals regulate cell growth, pathogenesis, and autophagy in ovarian cancer and melanoma. *Cancer Res* 2016;76:6964–74.
8 Zhang D, Reyes RM, Osta E, *et al*. Bladder cancer cell-intrinsic PD-L1 signals promote mTOR and autophagy activation that can be inhibited to improve cytotoxic chemotherapy. *Cancer Med* 2021;10:2137–52.
9 Wu X, Li Y, Liu X, *et al*. Targeting B7-H1 (PD-L1) sensitizes cancer cells to chemotherapy. *Heliyon* 2018;4:e01039.
10 Peng S, Wang R, Zhang X, *et al*. EGFR-TKI resistance promotes immune escape in lung cancer via increased PD-L1 expression. *Mol Cancer* 2019;18:165.
11 Gao Y, Nihira NT, Bu X, *et al*. Acetylation-dependent regulation of PD-L1 nuclear translocation dictates the efficacy of anti-PD-1 immunotherapy. *Nat Cell Biol* 2020;22:1064–75.
12 Hou J, Zhao R, Xia W, *et al*. PD-L1-mediated gasdermin C expression switches apoptosis to pyroptosis in cancer cells and facilitates tumour necrosis. *Nat Cell Biol* 2020;22:1264–75.
13 Shayegh A, Khalatbari F, Zonoubi N, *et al*. Chlorambucil-Chitosan Nano-conjugate: an efficient agent against breast cancer targeted therapy. *Curr Drug Deliv* 2021;18:721–8.
14 Sharman JP, Egyed M, Jurczak W, *et al*. Acalabrutinib with or without obinutuzumab versus chlorambucil and obinutuzmab for treatment-naive chronic lymphocytic leukaemia (ELEVATE TN): a randomised, controlled, phase 3 trial. *Lancet* 2020;395:1278–91.
15 Drerup JM, Deng Y, Pandeswara SL, *et al*. CD122-Selective IL2 complexes reduce immunosuppression, promote Treg fragility, and sensitize tumor response to PD-L1 blockade. *Cancer Res* 2020;80:5063–75.
16 Thibodeaux SR, Barnett BB, Pandeswara S, *et al*. IFNalpha augments clinical efficacy of regulatory T-cell depletion with Denileukin Diftitox in ovarian cancer. *Clin Cancer Res* 2021;27:3661–73.
17 Dou J, Pan M, Wen P, *et al*. Isolation and identification of cancer stem-like cells from murine melanoma cell lines. *Cell Mol Immunol* 2007;4:467–72.
18 Gil M, Komorowski MP, Seshadri M, *et al*. CXCL12/CXCR4 blockade by oncolytic virotherapy inhibits ovarian cancer growth by decreasing immunosuppression and targeting cancer-initiating cells. *J Immunol* 2014;193:5327–37.
19 Sato H, Jeggo PA, Shibata A. Regulation of programmed death-ligand 1 expression in response to DNA damage in cancer cells: implications for precision medicine. *Cancer Sci* 2019;110:3415–23.
20 Wang Y-J, Fletcher R, Yu J, *et al*. Immunogenic effects of chemotherapy-induced tumor cell death. *Genes Dis* 2018;5:194–203.
21 Turubanova VD, Balalaeva IV, Mishchenko TA, *et al*. Immunogenic cell death induced by a new photodynamic therapy based on photosens and photodithazine. *J Immunother Cancer* 2019;7:350.
22 Guo J, Yu Z, Sun D, *et al*. Two nanoformulations induce reactive oxygen species and immunogenetic cell death for synergistic chemo-immunotherapy eradicating colorectal cancer and hepatocellular carcinoma. *Mol Cancer* 2021;20:10.
23 Zitvogel L, Kepp O, Senovilla L, *et al*. Immunogenic tumor cell death for optimal anticancer therapy: the calreticulin exposure pathway. *Clin Cancer Res* 2010;16:3100–4.
24 Verma V, Jafarzadeh N, Boi S, *et al*. MEK inhibition reprograms $CD8^+$ T lymphocytes into memory stem cells with potent antitumor effects. *Nat Immunol* 2021;22:53–66.
25 Yachida N, Yoshihara K, Suda K, *et al*. Biological significance of KRAS mutant allele expression in ovarian endometriosis. *Cancer Sci* 2021;112:2020–32.

26 Ogishima J, Taguchi A, Kawata A, *et al*. The oncogene KRAS promotes cancer cell dissemination by stabilizing spheroid formation via the MEK pathway. *BMC Cancer* 2018;18:1201.
27 Hu X, Wang J, Chu M, *et al*. Emerging role of ubiquitination in the regulation of PD-1/PD-L1 in cancer immunotherapy. *Mol Ther* 2021;29:908–19.
28 Cha J-H, Chan L-C, Li C-W, *et al*. Mechanisms controlling PD-L1 expression in cancer. *Mol Cell* 2019;76:359–70.
29 Zhang J, Bu X, Wang H, *et al*. Cyclin D-CDK4 kinase destabilizes PD-L1 via cullin 3-SPOP to control cancer immune surveillance. *Nature* 2018;553:91–5.
30 Deng L, Qian G, Zhang S, *et al*. Inhibition of mTOR complex 1/p70 S6 kinase signaling elevates PD-L1 levels in human cancer cells through enhancing protein stabilization accompanied with enhanced β-TrCP degradation. *Oncogene* 2019;38:6270–82.
31 Wang S, Xu L, Che X, *et al*. E3 ubiquitin ligases Cbl-b and c-Cbl downregulate PD-L1 in EGFR wild-type non-small cell lung cancer. *FEBS Lett* 2018;592:621–30.
32 Li C-W, Lim S-O, Xia W, *et al*. Glycosylation and stabilization of programmed death ligand-1 suppresses T-cell activity. *Nat Commun* 2016;7:12632.
33 Ghosh S, Nataraj NB, Noronha A, *et al*. PD-L1 recruits phospholipase C and enhances tumorigenicity of lung tumors harboring mutant forms of EGFR. *Cell Rep* 2021;35:109181.
34 Gupta HB, Clark CA, Yuan B, *et al*. Tumor cell-intrinsic PD-L1 promotes tumor-initiating cell generation and functions in melanoma and ovarian cancer. *Signal Transduct Target Ther* 2016;1:16030-.
35 Kornepati AVR, Vadlamudi RK, Curiel TJ. Publisher correction: programmed death ligand 1 signals in cancer cells. *Nat Rev Cancer* 2022;22:190.
36 Liang J, Wang L, Wang C, *et al*. Verteporfin inhibits PD-L1 through autophagy and the STAT1-IRF1-TRIM28 signaling axis, exerting antitumor efficacy. *Cancer Immunol Res* 2020;8:952–65.
37 Lim S-O, Li C-W, Xia W, *et al*. Deubiquitination and stabilization of PD-L1 by CSN5. *Cancer Cell* 2016;30:925–39.
38 Hua S, Gu M, Wang Y, *et al*. Oxymatrine reduces expression of programmed death-ligand 1 by promoting DNA demethylation in colorectal cancer cells. *Clin Transl Oncol* 2021;23:750–6.
39 Wang Y, Wang H, Yao H, *et al*. Regulation of PD-L1: emerging routes for targeting tumor immune evasion. *Front Pharmacol* 2018;9:536.
40 Yao H, Lan J, Li C, *et al*. Inhibiting PD-L1 palmitoylation enhances T-cell immune responses against tumours. *Nat Biomed Eng* 2019;3:306–17.
41 Li S-M, Zhou J, Wang Y, *et al*. Recent findings in the posttranslational modifications of PD-L1. *J Oncol* 2020;2020:5497015.
42 Wu B, Sun X, Gupta HB, *et al*. Adipose PD-L1 modulates PD-1/PD-L1 checkpoint blockade immunotherapy efficacy in breast cancer. *Oncoimmunology* 2018;7:e1500107.
43 Song N, Bai M, Che X, *et al*. PD-L1 upregulation accompanied with epithelial-mesenchymal transition attenuates sensitivity to ATR inhibition in p53 mutant pancreatic cancer cells. *Med Oncol* 2020;37:47.
44 Feng D, Qin B, Pal K, *et al*. $BRAF^{V600E}$-induced, tumor intrinsic PD-L1 can regulate chemotherapy-induced apoptosis in human colon cancer cells and in tumor xenografts. *Oncogene* 2019;38:6752–66.
45 Sato H, Niimi A, Yasuhara T, *et al*. DNA double-strand break repair pathway regulates PD-L1 expression in cancer cells. *Nat Commun* 2017;8:1751.
46 Vendetti FP, Karukonda P, Clump DA, *et al*. ATR kinase inhibitor AZD6738 potentiates CD8+ T cell-dependent antitumor activity following radiation. *J Clin Invest* 2018;128:3926–40.
47 Decout A, Katz JD, Venkatraman S, *et al*. The cGAS-STING pathway as a therapeutic target in inflammatory diseases. *Nat Rev Immunol* 2021;21:548–69.
48 Borghaei H, Langer CJ, Paz-Ares L, *et al*. Pembrolizumab plus chemotherapy versus chemotherapy alone in patients with advanced non-small cell lung cancer without tumor PD-L1 expression: a pooled analysis of 3 randomized controlled trials. *Cancer* 2020;126:4867–77.
49 Zhang Y, Zhou H, Zhang L. Which is the optimal immunotherapy for advanced squamous non-small-cell lung cancer in combination with chemotherapy: anti-PD-1 or anti-PD-L1? *J Immunother Cancer* 2018;6:135.
50 Cubas R, Moskalenko M, Cheung J, *et al*. Chemotherapy combines effectively with anti-PD-L1 treatment and can augment antitumor responses. *J Immunol* 2018;201:2273–86.
51 Opzoomer JW, Sosnowska D, Anstee JE, *et al*. Cytotoxic chemotherapy as an immune stimulus: a molecular perspective on turning up the immunological heat on cancer. *Front Immunol* 2019;10:1654.
52 Dücker P, Hüning S, Rohde S, *et al*. [Merkel cell carcinoma in chronic lymphocytic leukemia: Successful treatment with PD-L 1 inhibition, avelumab and chlorambucil]. *Hautarzt* 2020;71:553–6.
53 Yu J, Qin B, Moyer AM, *et al*. Regulation of sister chromatid cohesion by nuclear PD-L1. *Cell Res* 2020;30:590–601.
54 Zhang W, Jin J, Wang Y, *et al*. PD-L1 regulates genomic stability via interaction with cohesin-SA1 in the nucleus. *Signal Transduct Target Ther* 2021;6:81.